RSC Advances

PAPER

View Article Online
View Journal | View Issue

Cite this: *RSC Adv.*, 2018, **8**, 10089

Effects of multiwalled carbon nanotubes on CH_4 hydrate in the presence of tetra-*n*-butyl ammonium bromide

Dong-Liang Li,[abcd] Shu-Mei Sheng,[abcde] Ye Zhang,[abcde] De-Qing Liang *[abcd] and Xiao-Ping Wu[f]

Hydrate formation is an important technology for gas storage and transportation. In this work, the effect of multiwalled carbon nanotubes (MWCNTs) on CH_4 hydrate formation was examined by determining the phase equilibrium conditions and kinetics characteristics of a mixed system of CH_4, tetra-*n*-butyl ammonium bromide (TBAB), and MWCNTs. The phase equilibrium was examined in the temperature range of 286.13–293.04 K and the pressure range of 0.55–6.56 MPa for various mass fractions of MWCNTs (0.004, 0.1, 0.5, and 1.0 wt%). In the CH_4 + TBAB system, the presence of MWCNTs was found to shift the phase equilibrium conditions to a lower temperature by about 1 K compared with those in the absence of MWCNTs. However, the concentration of MWCNTs had little effect on the phase equilibrium conditions. When the concentration of MWCNTs was 1.0 wt%, the addition of MWCNTs reduced the induction time of hydrate formation by 79.5%. When the concentration of MWCNTs was 0.1 wt%, the addition of MWCNTs enhanced the hydrate growth rate by 61.5%. Powder X-ray diffraction patterns revealed that hydrates with orthorhombic structures (corresponding to TBAB·38H_2O with 3D cages) were formed in the systems with and without MWCNTs. Moreover, peaks corresponding to MWCNTs were not observed in the patterns of the hydrates and the addition of MWCNTs had no influence on the structure and type of hydrate. Thus, MWCNTs were not incorporated into the hydrate cages.

Received 5th February 2018
Accepted 6th March 2018

DOI: 10.1039/c8ra01124a

rsc.li/rsc-advances

1. Introduction

Natural gas hydrates or gas hydrates are ice-like crystalline solids composed of water molecules (host) and gas molecules (guest) that exist at certain temperatures and pressures. In these hydrates, gas molecules, such as CH_4, CO_2, N_2, and H_2, are caged in water molecule cavities that are connected by hydrogen bonds. There are three common hydrate structures: structure I (sI), structure II (sII), and structure H (sH), which depend on the size and nature of the gas molecules.[1,2] In 1940, Fowler *et al.* found that some quaternary ammonium salts could form hydrates at room temperature and atmospheric pressure.[3] Subsequently, Jeffrey determined X-ray crystal structures of this kind of hydrate and found that the cages were composed of both water molecules and anions.[4] These types of organic hydrates have been termed as semiclathrate hydrates. Recently, many researchers have focused on semiclathrate hydrates owing to their possible applications in gas storage and transportation, gas separation, *etc.*[5–8]

Hydrate technology, as an emerging approach for solidifying natural gas, is considered an alternative to liquefied natural gas (LNG) or compressed natural gas (CNG) technologies for natural gas storage and transportation.[9] The application of hydrate technology to gas storage and transportation has several advantages compared with CNG and LNG, including lower cost, improved safety, and higher efficiency.[10,11] However, there are several technical problems that restrict the industrial application of hydrate technology, such as the long induction time for hydrate formation, the slow rate of hydrate formation, and the low temperature and high pressure conditions required for hydrate formation. In order to overcome these bottlenecks, researchers have developed physical methods, including stirring, bubbling, and spraying,[12–14] and chemical methods, including adding surfactants such as tetrahydrofuran (THF), tetra-*n*-butyl ammonium bromide (TBAB), cyclopentane (CP), and sodium dodecyl sulfate (SDS).[15–20] These methods have made obvious

[a]*Guangzhou Institute of Energy Conversion, Chinese Academy of Sciences, Guangzhou 510640, China*
[b]*CAS Key Laboratory of Gas Hydrate, Guangzhou 510640, China*
[c]*Guangdong Provincial Key Laboratory of New and Renewable Energy Research and Development, Guangzhou 510640, China*
[d]*Guangzhou Center for Gas Hydrate Research, Chinese Academy of Sciences, Guangzhou 510640, China. E-mail: liangdq@ms.giec.ac.cn; Fax: +86 20870576 69*
[e]*Nano Science and Technology Institute, University of Science and Technology of China, Suzhou 215123, China*
[f]*School of Earth and Space Sciences, University of Science and Technology of China, Hefei 230026, China*

contributions, but cannot meet the requirements for industrial application of hydrate technology.

Nanofluids, which have efficient thermal conductivity, have been applied to hydrate technology to reduce the induction time of hydrate formation.[9,21] The addition of nano-copper to HFC134a (CH_3FCF_3) gas hydrates (sII) was first reported by Li *et al.*[22] The results indicated that the addition of nano-copper particles promoted not only mass transfer but also heat transfer during the formation and dissociation of HFC134a hydrates, that is, the presence of nano-copper made it faster to form hydrates. Park *et al.*[23] examined the effect of low mass fractions of multiwalled carbon nanotubes (MWCNTs) (0.001, 0.002, 0.003, 0.004, 0.005, and 0.006 wt%) on CH_4 hydrate (sI). The results showed that the phase equilibrium curve shifted to higher temperatures by about 1 K relative to the pure water system and the induction time decreased remarkably. Moreover, an increase of nearly 300% in the amount of gas consumed was observed at an MWCNT concentration of 0.004 wt%. Yu *et al.*[24] investigated the effect of graphite nanoparticles on the phase equilibrium of CO_2 hydrate (sI). They concluded that the presence of nanoparticles shifted the equilibrium curves to lower temperatures by about 1 K, but the concentration of nanofluids had no effect on the phase equilibrium. Lim *et al.*[25] studied the CH_4 + THF + oxidized multiwalled carbon nanotubes (OMWCNTs) system and found that OMWCNTs had no effect on the phase equilibrium, both in pure water and in THF aqueous solution (sII). However, the presence of THF and OMWCNTs increased the amount of gas consumed by up to 5.2 times compared with that in the pure water system at 3.4 K subcooling and also decreased the induction time of hydrate formation considerably. All these studies confirmed that nanofluids have a positive effect on the induction time of hydrate formation. However, there is no agreement on the shift of the phase equilibrium curves. According to the experimental results in the literature, we conjecture that the effect of MWCNTs on the phase equilibrium conditions may be related to the type of gas or the structure of the hydrate. However, to the best of our knowledge, phase equilibrium data related to the effect of MWCNTs on semiclathrate hydrates is not available in the literature.

In this work, we conducted a series of experiments to examine CH_4 hydrate in TBAB aqueous solution in the presence of different mass fractions of MWCNTs (0.0, 0.004, 0.1, 0.5, and 1.0 wt%). The concentration of TBAB was 38.5 wt% in accordance with the literature.[26,27] The purpose of this work was to elucidate the effects of MWCNTs on the phase equilibrium and the formation dynamics of semiclathrate hydrates, and provide fundamental data that can be applied to gas storage and transportation applications.

2. Experimental section

2.1 Materials

CH_4 (99.9% purity, Guangzhou Yigas Gases Co. Ltd.) and TBAB (>98.0% purity, Tokyo Chemical Industry, Japan) were used in these experiments. The MWCNTs used in this study (95% purity, bulk density of 0.1 g cm^{-3}, Tokyo Chemical Industry, Japan) were tubular in shape with diameters of <10 nm, lengths of 5–15 μm, and surface areas of 100–160 m^2 g^{-1}. To prepare the solutions, TBAB and MWCNTs were weighed using an electronic balance with an uncertainty of ±0.1 mg. Deionized water with a resistivity of 18 MΩ cm was obtained in the laboratory.

2.2 Treatment and characterization of pristine MWCNTs

2.2.1. Treatment of pristine MWCNTs. Defined amounts of MWCNTs and TBAB were weighed then added into a defined volume of deionized water. Then, the suspension was shaken for 30 min using a vortex mixer to achieve good dispersity. The suspension was then left undisturbed for a defined time.

2.2.2. Characterization of pristine MWCNTs. A cryo-scanning electron microscope (Hitachi, S34800) was used to observe the morphology of the pristine MWCNTs at room temperature. A X-ray diffraction (XRD) pattern (2θ range of 5–90°) of the MWCNTs was determined using a powder X-ray diffraction (PXRD) spectrometer (PANalytical, X'Pert Pro MPD) at room temperature.

2.3 Experimental apparatus

A schematic of the apparatus used in this work is shown in Fig. 1. The apparatus comprised two cylindrical vessels made of #316 stainless steel, each with a total volume of 100 mL and a maximum work pressure of 25 MPa. The vessels were immersed in a thermostatic bath (Tian Heng THD-2030). The inner temperature and pressure of each vessel were monitored using a platinum resistance thermometer (PT100) with a precision of ±0.1 K and a pressure transducer (CYB-20S) with a precision of ±0.02 MPa, respectively. The aqueous solutions inside the cells were driven by a magnetic stirrer (Mei Ying Pu 98-2) throughout the experiments. The experimental temperature and pressure data were collected every 10 s using an Agilent data acquisition system and saved to a computer.

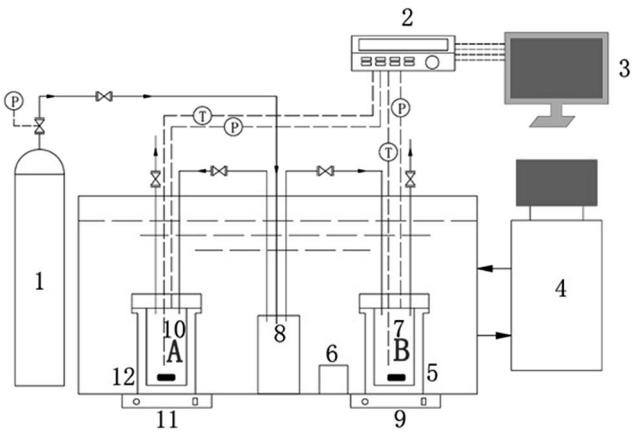

Fig. 1 Schematic diagram of the experimental apparatus. (1) Gas cylinder; (2) data acquisition; (3) personal computer; (4) thermostatic bath; (5) and (12) stirrers; (6) subaqueous pump; (7) and (10) reactors; (8) gas buffer tank; (9) and (11) magnetic stirrer apparatus; P, pressure transducer; T, temperature sensor.

2.4 Experimental procedure

2.4.1. Phase equilibrium. The dissociation conditions of the hydrates were measured using the isochoric pressure-search method.[28–33] First, the required solution or suspension was prepared. According to the concentrations required, defined amounts of MWCNTs and TBAB were weighed and then added into a defined volume of deionized water. Then, the suspension was shaken for 30 min using a vortex mixer to achieve good dispersity.

Before each experiment, the vessel was washed with deionized water once and then with the experimental suspension three times. The vessel was charged with approximately 30 mL of the experimental suspension and then the air in the system was evacuated using a vacuum pump. After setting the initial temperature of the thermostatic bath to 298.15 K, the desired pressure of CH_4 gas was introduced into the buffer tank. When the gas temperature was stable, the magnetic stirrer was turned on at a speed of 600 rpm and the vessel was pressurized to the initial desired pressure. The temperature of the thermostatic bath was set to a lower value (ensuring that the subcooling temperature exceeded 10 K) to form the hydrate. During the cooling process, a sharp decrease in pressure along with a sudden increase in temperature indicated the formation of the hydrate. In order to form a sufficient amount of hydrate, the bath was maintained at a stable temperature for 4 h. Subsequently, the temperature of the system was increased gradually by controlling the temperature of the thermostatic bath. Initially, the temperature was increased in large steps. Once the pressure increased steeply, indicating the beginning of hydrate dissociation, the temperature was increased in steps of 0.1 K, with each temperature maintained for 4 h to achieve an equilibrium state. After dissociation of the hydrate was complete, the temperature was increased in steps of 0.2 K. Finally, the pressure–temperature (P–T) diagram of hydrate formation and dissociation was plotted. The point at which the slope of the P–T curve sharply changed was considered as the hydrate dissociation point.[32,34,35]

2.4.2. Dynamics. Solutions or suspensions were prepared as described for the phase equilibrium experiments. Before each experiment, the vessel was charged with 30 mL of the experimental suspension and then air was evacuated using a vacuum pump. At first, the temperature was maintained at 303.15 K for 1 h. Then the reactor was pressurized with experimental gas to 5.5 MPa. Subsequently, the temperature was reduced to the required value to obtain a subcooling of 6 K. A sharp decrease in the pressure curve along with a sudden increase in the temperature curve indicated the formation of the hydrate. The temperature and pressure were kept constant after the water was mostly converted into hydrates. Then the dynamics experiment was terminated. The sample was stirred during the experiment. Each experiment was repeated five times, with the temperature maintained at >300 K for more than 4 h after each experiment to eliminate the "memory effect".[36]

In this study, the induction time was defined as the time that elapses from the moment the initial equilibrium state is formed to the time a certain detectable number of hydrate-forming gas molecules are consumed.[37] Fig. 2 and 3 show the cooling curve and the change in temperature and pressure over time for 1.0 wt% MWCNTs at 5.5 MPa with a subcooling of 6 K, respectively. The time elapsed between points A and B is defined as the induction time in Fig. 2 which corresponds to the time between C and D in Fig. 3.

Molar gas consumption rates can be obtained according to the following equation:

$$r = \mathrm{d}n/\mathrm{d}t \quad (1)$$

where dn is the change in moles of gas over a specific period and dt is the duration of this period. A period of 600 s was selected to calculate the molar gas consumption, as the slope was almost constant over this time.

The method of calculating the amount of gas consumed was introduced in a previous report.[38] The volume of gas in the reactor is assumed to be constant. Therefore, the consumption of methane gas to form the hydrate is related to the pressure drop. The total amount of gas consumed at time t is determined using the following equation.

$$n = \frac{P_0 V}{Z_0 R T_0} - \frac{PV}{ZRT} \quad (2)$$

where P and T are the pressure and temperature at time t; P_0 and T_0 are the pressure and temperature at the initial time, $t = 0$; V is the volume of gas in the reactor; R is the molar gas constant; and Z is the compressibility factor, which can be calculated using the Peng–Robinson equation of state.[39] Using the temperature and pressure data collected in the dynamics experiments, we can calculate the amount of gas consumed for the systems examined in this study.

2.4.3. PXRD analysis. XRD patterns (2θ range of 5–90°) of the gas hydrates were determined using a PXRD spectrometer (PANalytical, X'Pert Pro MPD) at 173.15 K and atmospheric pressure. After a dramatic drop in pressure during cooling of the sample in a high-pressure cell, the pressure stabilized. When a stable pressure was maintained for more than 10 h, the water in the high-pressure cell was considered to have been mostly transformed into a hydrate. The hydrate crystals in the

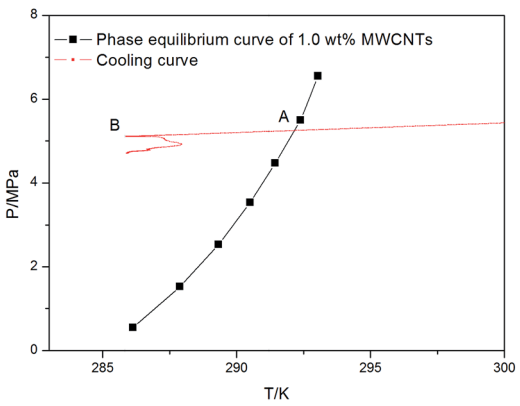

Fig. 2 The cooling curve for 1.0 wt% MWCNTs at 5.5 MPa and a subcooling of 6 K.

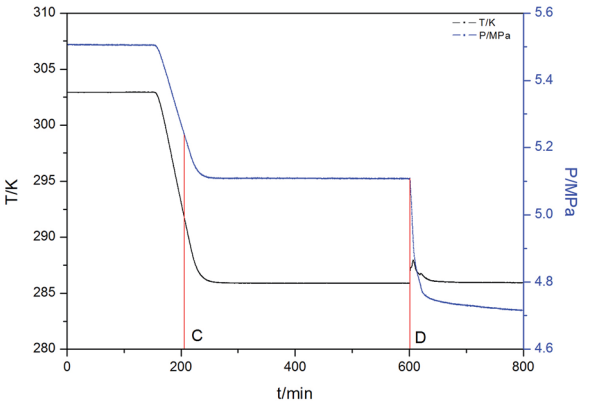

Fig. 3 The change in temperature and pressure over time for 1.0 wt% MWCNTs at 5.5 MPa and a subcooling of 6 K.

high-pressure cell were then taken out and ground (in a liquid nitrogen vessel) into small particles with an average diameter of approximately 50 μm. The ground hydrate crystals were stored in liquid nitrogen for the PXRD experiments.

3. Results and discussion

3.1 Characterization of MWCNTs

3.1.1. Stability of nanotube suspensions. Fig. 4 shows a dispersion of 0.1% MWCNTs in TBAB solution. After mixing, there was no noticeable deposition during the first 10 min but complete deposition of the MWCNTs was observed after 3 h. Song *et al.*[40] treated pristine MWCNTs with a sonicator and observed complete deposition after 30 min. As a result, vortex mixing achieved greater dispersion than sonication. Thus, in this study, the samples were stirred during the entire experimental process to maintain good dispersity of MWCNTs in solution.

3.1.2. Scanning electron microscopy (SEM). The morphology of the MWCNTs was examined SEM (Fig. 5). The SEM images reveal individual nanotubes as well as entangled nanotube structures. As a result, the MWCNTs may be easily agglomerated at high concentrations.

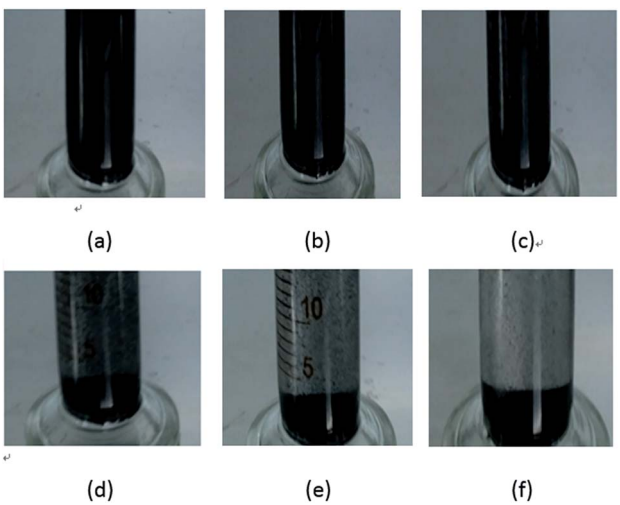

Fig. 4 Changes in a nanotube dispersion in TBAB solution over time. (a) After 0 min; (b) after 5 min; (c) after 10 min; (d) after 30 min; (e) after 60 min; (f) after 180 min.

3.2 Phase equilibrium

The validity of the experimental apparatus and the method applied to acquire phase equilibrium data were checked by comparing the $CH_4 + H_2O$ phase equilibrium data with literature data.[30,41,42] Table 1 lists the phase equilibrium data for CH_4 hydrate in pure water. As shown in Fig. 6, the equilibrium pressures and temperatures obtained in this work are in good agreement with the literature values, indicating that the apparatus and method applied in this study are reliable.

The phase equilibrium data for CH_4 + 38.5 wt% TBAB + MWCNTs (0.004, 0.1, 0.5, and 1.0 wt%) are shown in Fig. 7. The phase equilibrium data for CH_4 + 38.5 wt% TBAB are found in the literature.[26] The data obtained as the average of three measurements are presented in Table 2. As shown in Fig. 7, compared with the CH_4 + 38.5 wt% TBAB system, a significant upward shift in the formation pressure of the CH_4 and TBAB semiclathrate is observed at each temperature for the CH_4 + 38.5 wt% TBAB + MWCNTs systems. This result means that the pressure required for hydrate formation in nanoparticle suspensions is higher than that in TBAB aqueous solution. In other words, the nanoparticles have

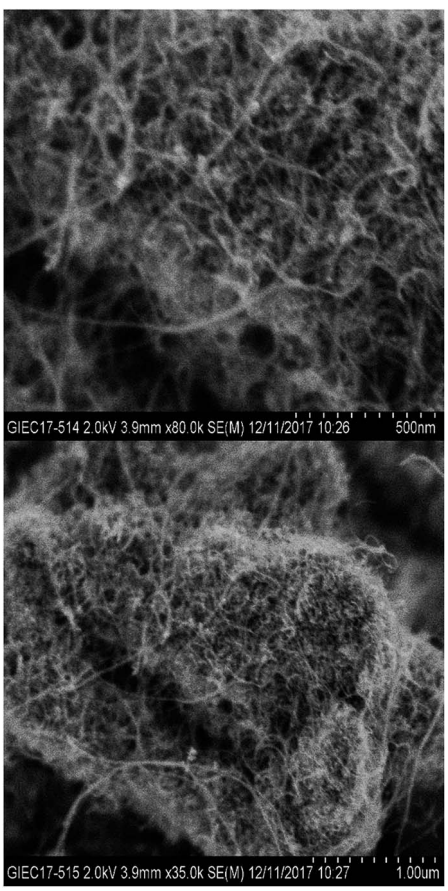

Fig. 5 SEM images of pristine MWCNTs.

Table 1 Phase equilibrium data for CH_4 hydrate in pure water

T/K	P/MPa
281.5	6.05
281.8	6.25
283.1	7.11
284.5	8.41
285.6	9.56

a negative effect on the thermodynamics of gas hydrate formation.

Similar to the CO_2 and graphite nanoparticle suspension system,[24] this phenomenon can be explained as follows. MWCNTs in water increase the disorder of the water molecules, which results in an increase of the system entropy. Hence, the formation of hydrate crystal cavities requires more hydrogen bond energy, which leads to an increase of the temperature and pressure of hydrate formation. In addition, some larger MWCNTs have tubular structures that can reduce the activity of water and increase the pressure of hydrate formation. However, our result does not agree with the conclusions reported for the CH_4 + MWCNTs suspension system (sI).[25] In fact, the hydrate structure for the CH_4 + 38.5 wt% TBAB + MWCNTs systems was different from that of the CH_4 + MWCNTs suspension system. As a result, the thermodynamic function of the MWCNTs may be related to the type of gas and hydrate.

As shown in Fig. 7, the concentration of MWCNTs had little effect on the phase equilibrium of gas hydrate formation. In order to show this phenomenon clearly, the phase equilibrium data are plotted as a function MWCNT concentration in Fig. 8. As shown, the equilibrium conditions do not exhibit a gradual shift with increasing MWCNT concentration. Instead, an abrupt change is observed at a low MWCNT concentration (0.004 wt%). These results are in agreement with those in different porous media, such as nano-copper,[22] graphite nanoparticles,[24] silica gel,[43] and porous glass.[44] However, the existence of agglomerated MWCNTs owing to van der Waals interactions between the nanotubes makes the dispersion of MWCNTs in matrices difficult, limiting their solubility in water.[45] As described previously, dissolved MWCNTs increase the system entropy by

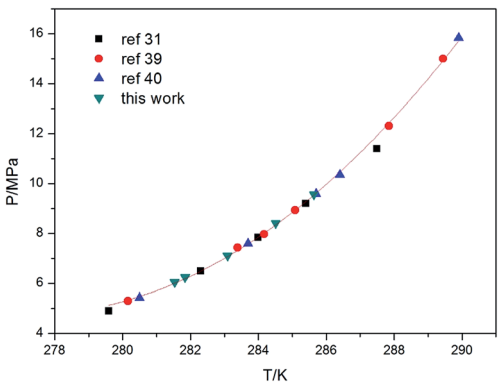

Fig. 6 Comparison of the phase equilibrium data for CH_4 hydrate in pure water obtained in this work with literature data.

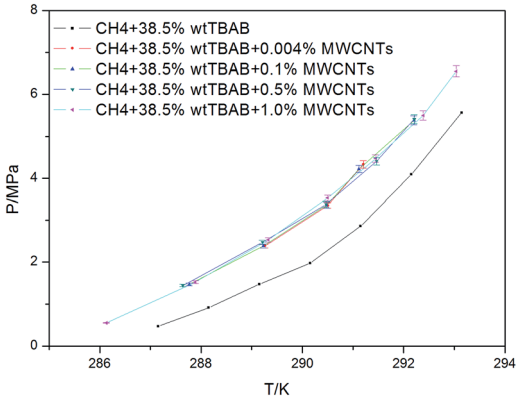

Fig. 7 Phase equilibrium data for CH_4 + 38.5 wt% TBAB at different MWCNT concentrations.

increasing the disorder of the water molecules. Thus, more hydrogen bond energy is required for hydrate crystal cavity formation, which increases the pressure of hydrate formation.[24,46] However, once the MWCNT mass fraction is larger than the maximum solubility of MWCNTs, increasing the mass fraction further has a negligible influence on the system.

3.3 Induction time and gas consumption rate

Fig. 9 shows the induction times for different MWCNT concentrations (0.0, 0.004, 0.008, 0.1, and 1.0 wt%) at a subcooling of 6 K and a pressure of 5.5 MPa. Although there is an uncertainty in the induction time of each experimental group, we found that the presence of MWCNTs reduces the induction time obviously compared with the system without MWCNTs at the same subcooling. For example, the average induction time of the control system is 968.4 min, whereas the induction time of the system with 1.0 wt% MWCNTs is 198.2 min. Thus, in this

Table 2 Phase equilibrium data for CH_4 + 38.5 wt% TBAB + MWCNTs

w_{MWCNTs}/wt%	T/K	P/MPa
0.004	289.26	2.39
	290.51	3.36
	291.21	4.33
0.1	287.77	1.47
	289.23	2.39
	290.48	3.36
	291.12	4.22
	292.20	5.38
0.5	287.64	1.45
	289.21	2.48
	290.47	3.38
	291.47	4.41
	292.21	5.41
1.0	286.13	0.55
	287.89	1.52
	289.33	2.53
	290.50	3.53
	291.45	4.47
	292.39	5.50
	293.04	6.56

case, the presence of MWCNTs shortened the hydrate formation time by 79.5%. Generally, the average induction time decreased as the concentration of MWCNTs increased, except in the case of 0.1 wt% MWCNTs. This discrepancy can be explained by the uncertainty in the induction time. The results of our experiment agreed with the conclusions of other studies.[22,47] Methane hydrate nucleation is an exothermic process. This process is faster when the heat is dissipated, and carbon nanotubes have been found to have good thermal conductivity.[9,48] In addition, the presence of MWCNTs increases the surface area for nucleation sites for hydrate formation.[49] Furthermore, heterogeneous nucleation is more likely to occur than homogenous nucleation.[50] Therefore, nucleation of methane hydrate is easier and faster in the presence of MWCNTs.

Fig. 10 shows that the average growth rates of the systems with MWCNTs are higher than that of the control system (1.17×10^{-5} mol s^{-1}). The average gas consumption rate was 1.50×10^{-5} mol s^{-1} at 0.004 wt% MWCNTs, and as the concentration of MWCNTs increased, the average gas consumption rate first increased to a maximum of 1.89×10^{-5} mol s^{-1} at 0.1 wt% MWCNTs and then decreased to 1.62×10^{-5} mol s^{-1} at 1.0 wt% MWCNTs. Pasieka *et al.* investigated the effect of hydrophobic and hydrophilic MWCNTs on methane hydrate growth kinetics.[51] They found that the methane hydrate growth rate increased with increasing concentrations of hydrophobic MWCNTs and then reached a plateau. Further, at low hydrophilic MWCNT loadings, the growth rate sharply increased by 16.34% at 0.1 ppm MWCNTs, then rapidly decreased to the baseline value at 1 ppm MWCNTs, and then increased almost linearly with increasing MWCNT concentration. However, all these experiments were conducted at low MWCNT concentrations (≤10 ppm). In this work, with the increase of the concentration of carbon nanotubes, the growth rate of methane hydrate firstly increases and then decreases. Renault-Crispo *et al.* recently investigated the CO_2 + TBAB + oxygen-functionalized multi-walled carbon nanotubes (OMWCNTs) system.[52] They showed that the addition of OMWCNTs could enhance the gas consumption rate of the TBAB gas hydrate system when the induction time was short and when the induction time was more than 1 h, the average gas consumption rate of the systems with and without OMWCNTs were not statistically different. In this work, however, it was not found the regular conclusion between average gas consumption rate and induction time.

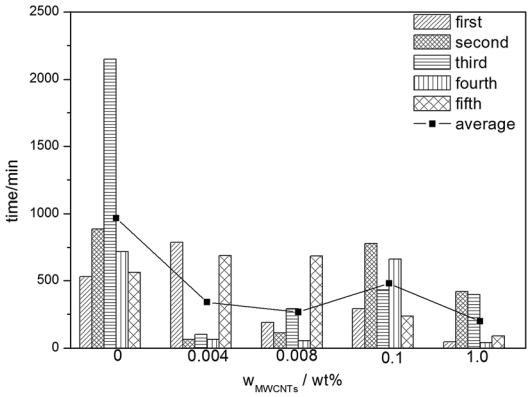

Fig. 9 Induction times for different MWCNT concentrations at a subcooling of 6 K and a pressure of 5.5 MPa.

3.4 PXRD analysis

Fig. 11 shows the PXRD patterns of CH_4 hydrates formed in the absence and presence of different concentrations of MWCNTs, pure CH_4 hydrate, and pristine MWCNTs. The PXRD patterns of all the hydrate samples are consistent with orthorhombic *Pmma* structures.[53,54] The peaks at $2\theta = 7.11°$, 8.57°, 11.1°, 16.4°, 17.2°, and 18.4° were assigned to Miller indices (*h k l*) of 010, 200, 210, 220, 202, and 401, respectively. In the PXRD pattern of pristine MWCNTs, the peaks at $2\theta = 25.85°$ and 43.43° were assigned to the Miller indices (*h k l*) of 002 and 100.[55,56] In Fig. 11, asterisks indicate the peaks corresponding to pure CH_4 hydrate. Judging from the PXRD pattern and the conditions required for methane hydrate formation, there is no pure methane hydrate in the semiclathrate systems. As shown by the red dotted line in Fig. 11, there is no apparent MWCNT peak in the hydrate systems containing MWCNTs. According to the PXRD analysis, MWCNTs may not participate in the construction of the hydrate cavities and have no effect on the type of TBAB + CH_4 hydrate

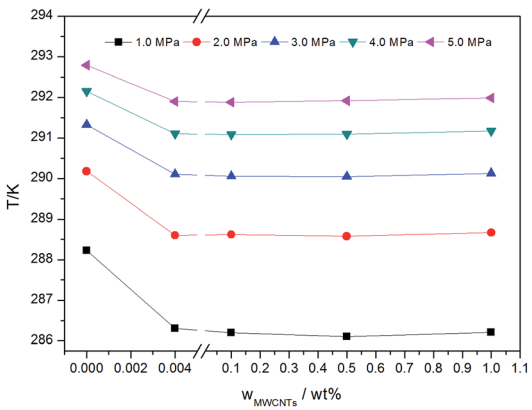

Fig. 8 CH_4 hydrate dissociation conditions for different MWCNT concentrations at various pressures.

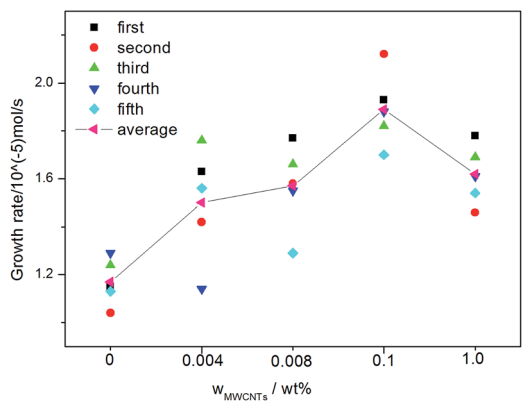

Fig. 10 Growth rates of hydrate systems at different MWCNT concentrations.

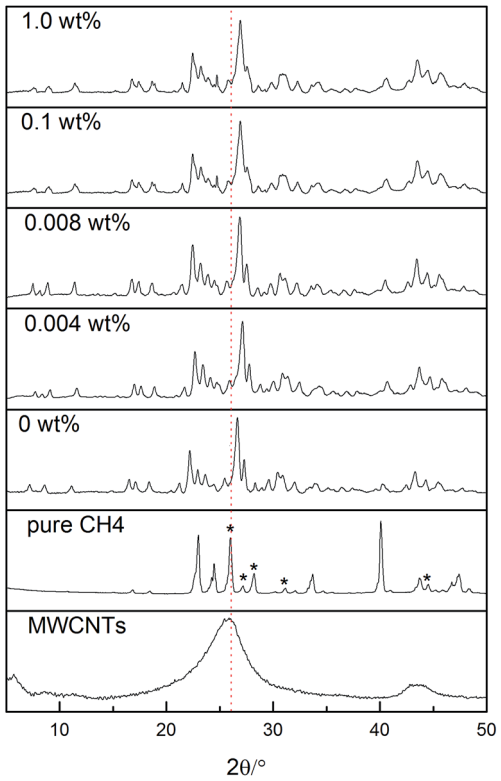

Fig. 11 PXRD patterns of CH_4 hydrates with and without MWCNTs and pristine MWCNTs. The asterisks indicate peaks corresponding to pure CH_4 hydrate.

formed. Microinteractions between the hydrate crystals and MWCNTs, as well as those between MWCNTs, only influence the thermal conductivity and the activity of the suspension.

4. Conclusion

This paper has presented the effects of adding MWCNTs to a CH_4 + TBAB system on CH_4 hydrate formation. The presence of MWCNTs reduced the induction time. Moreover, the phase equilibrium conditions for CH_4 hydrates were shifted to lower temperatures by about 1 K in the presence of MWCNTs relative to the CH_4 + TBAB system. However, above a concentration of 0.004 wt%, the presence of MWCNTs had no significant effect on the phase equilibrium conditions. The PXRD patterns showed that the semiclathrate hydrates formed in the absence and presence of MWCNTS both had orthorhombic structures. Moreover, MWCNTs were likely not involved in the construction of the hydrate cavities. Thus, the microinteractions that exist between the hydrate crystals and the MWCNTs, as well as between MWCNTs, only influenced the thermal conductivity and the activity of the suspension. Therefore, the addition of MWCNTs is an effective way of increasing the speed of hydrate formation without affecting the structure of hydrate.

Conflicts of interest

There are no conflicts to declare.

Acknowledgements

The work was supported by the National Natural Science Foundation of China (51474197 and 51661165011) and the National Key Research and Development Plan of China (No. 2016YFC0304002).

References

1 E. D. Sloan, *Clathrate Hydrates of Natural Gas*, ed. M. Dekker, 1998.
2 E. D. Sloan Jr, *Nature*, 2003, **426**, 353–359.
3 D. L. Fowler, W. V. Loebenstein, D. B. Pall and C. A. Kraus, *J. Am. Chem. Soc.*, 1940, **62**, 1140–1142.
4 G. A. Jeffrey, *Acc. Chem. Res.*, 1969, **2**, 344–352.
5 N. Mayoufi, D. Dalmazzone, A. Delahaye, P. Clain, L. Fournaison and W. Fürst, *J. Chem. Eng. Data*, 2011, **56**, 2987–2993.
6 L. Shi and D. Liang, *J. Chem. Eng. Data*, 2015, **60**, 2749–2755.
7 L. L. Shi and D. Q. Liang, *Fluid Phase Equilib.*, 2015, **386**, 149–154.
8 L. P. Sales Silva, D. Dalmazzone, M. Stambouli, P. Arpentinier, A. Trueba and W. Fürst, *J. Chem. Thermodyn.*, 2016, **102**, 293–302.
9 L. Dongliang, P. Hao and L. Deqing, *Int. J Heat Mass Transfer*, 2017, **104**, 566–573.
10 H. Kanda, *Economic Study on Natural Gas Transportation with Natural Gas Hydrate (NGH) Pellets. 23rd world gas conference*, Amsterdam, 2006.
11 S. Y. Lee and G. D. Holder, *Fuel Process. Technol.*, 2001, **71**, 181–186.
12 M. Yang, W. Jing, P. Wang, L. Jiang and Y. Song, *Fluid Phase Equilib.*, 2015, **401**, 27–33.
13 P. Linga, R. Kumar, J. D. Lee, J. Ripmeester and P. Englezos, *Int. J. Greenhouse Gas Control*, 2010, **4**, 630–637.
14 Y. T. Luo, J. H. Zhu, S. S. Fan and G. J. Chen, *Chem. Eng. Sci.*, 2007, **62**, 1000–1009.
15 E. Brown, M. N. Khan, D. Salmin, J. Wells, S. L. Wang, C. J. Peters and C. A. Koh, *J. Nat. Gas Sci. Eng.*, 2016, **35**, 1435–1440.
16 D. Mech, G. Pandey and J. S. Sangwai, *Fluid Phase Equilib.*, 2015, **402**, 9–17.
17 D. Mech and J. S. Sangwai, *J. Chem. Eng. Data*, 2016, **61**, 3607–3617.
18 D. Posteraro, J. Pasieka, M. Maric and P. Servio, *J. Nat. Gas Sci. Eng.*, 2016, **35**, 1579–1586.
19 M. J. Yang, W. Jing, P. F. Wang, L. Jiang and Y. C. Song, *Fluid Phase Equilib.*, 2015, **401**, 27–33.
20 N. Ye and P. Zhang, *J. Chem. Eng. Data*, 2014, **59**, 2920–2926.
21 M. T. Pettes and L. Shi, *Adv. Funct. Mater.*, 2009, **19**, 3918–3925.
22 J. P. Li, D. Q. Liang, K. H. Guo, R. Z. Wang and S. S. Fan, *Energy Convers. Manage.*, 2006, **47**, 201–210.
23 S.-S. Park, S.-B. Lee and N.-J. Kim, *J. Ind. Eng. Chem.*, 2010, **16**, 551–555.
24 Y. S. Yu, S. D. Zhou, X. S. Li and S. L. Wang, *Fluid Phase Equilib.*, 2016, **414**, 23–28.

25 S.-H. Lim, S. B. Riffat, S.-S. Park, S.-J. Oh, W. Chun and N.-J. Kim, *Int. J. Energy Res.*, 2014, **38**, 374–379.
26 D. Li, J. Du, S. Fan, D. Liang, X. Li and N. S. Huang, *J. Chem. Eng. Data*, 2007, **52**, 1916–1918.
27 H. Oyama, W. Shimada, T. Ebinuma, Y. Kamata, S. Takeya, T. Uchida, J. Nagao and H. Narita, *Fluid Phase Equilib.*, 2005, **234**, 131–135.
28 B. Tohidi, R. W. Burgass, A. Danesh, K. K. Østergaard and A. C. Todd, *Ann. N. Y. Acad. Sci.*, 2000, **912**, 924–931.
29 Y. J. Lee, T. Kawamura, Y. Yamamoto and J. H. Yoon, *J. Chem. Eng. Data*, 2015, **57**, 3543–3548.
30 W.-Z. Wu, J.-A. Guan, X.-D. Shen, L.-L. Shi, Z. Long, X.-B. Zhou and D.-Q. Liang, *J. Chem. Eng. Data*, 2016, **61**, 3498–3503.
31 X.-D. Shen, Z. Long, L.-l. Shi and D.-Q. Liang, *J. Chem. Eng. Data*, 2015, **60**, 3392–3396.
32 Z. Long, X. Zhou, D. Liang and D. Li, *J. Chem. Eng. Data*, 2015, **60**, 2728–2732.
33 X. Long, Y. Wang, X. Lang, S. Fan and J. Chen, *J. Chem. Eng. Data*, 2016, **61**, 3897–3901.
34 Z. T. Ward, C. E. Deering, R. A. Marriott, A. K. Sum, E. D. Sloan and C. A. Koh, *J. Chem. Eng. Data*, 2015, **60**, 403–408.
35 L.-L. Shi, D.-Q. Liang and D.-L. Li, *J. Chem. Thermodyn.*, 2014, **68**, 322–326.
36 Q. Wu and B. Zhang, *J. Nat. Gas Chem.*, 2010, **19**, 446–451.
37 S.-D. Zhou, Y.-S. Yu, M.-M. Zhao, S.-L. Wang and G.-Z. Zhang, *Energy Fuels*, 2014, **28**, 4694–4698.
38 X.-D. Shen, L.-L. Shi, Z. Long, X.-B. Zhou and D.-Q. Liang, *J. Mol. Liq.*, 2016, **223**, 672–677.
39 D. Y. Peng and D. B. Robinson, *Ind. Eng. Chem. Fundam.*, 1976, **15**, 92–94.
40 Y. Song, F. Wang, G. Liu, S. Luo and R. Guo, *Energy Fuels*, 2017, **31**, 1850–1857.
41 J. Nixdorf and L. R. Oellrich, *Fluid Phase Equilib.*, 1997, **139**, 325–333.
42 A. H. Mohammadi, R. Anderson and B. Tohidi, *AIChE J.*, 2005, **51**, 2825–2833.
43 W. Zhang, J. W. Wilder and D. H. Smith, *J. Phys. Chem. B*, 2003, **107**, 13084–13089.
44 T. Uchida, T. Ebinuma, S. Takeya, A. Jiro Nagao and H. Narita, *J. Phys. Chem. B*, 2002, **106**, 820–826.
45 C. H. Park, E. Tocci, E. Fontananova, M. A. Bahattab, S. A. Aljlil and E. Drioli, *J. Membr. Sci.*, 2016, **514**, 195–209.
46 S.-P. Kang, J.-W. Lee and H.-J. Ryu, *Fluid Phase Equilib.*, 2008, **274**, 68–72.
47 S. Arjang, M. Manteghian and A. Mohammadi, *Chem. Eng. Res. Des.*, 2013, **91**, 1050–1054.
48 M. Xing, J. Yu and R. Wang, *Int. J. Heat Mass Transfer*, 2015, **88**, 609–616.
49 H. Najibi, M. M. Shayegan and H. Heidary, *J. Nat. Gas Sci. Eng.*, 2015, **23**, 315–323.
50 D. Kashchiev and A. Firoozabadi, *J. Cryst. Growth*, 2002, **243**, 476–489.
51 J. Pasieka, S. Coulombe and P. Servio, *Chem. Eng. Sci.*, 2013, **104**, 998–1002.
52 J.-S. Renault-Crispo, S. Coulombe and P. Servio, *Energy*, 2017, **128**, 414–420.
53 M. Oshima, M. Kida and J. Nagao, *J. Chem. Eng. Data*, 2016, **61**, 3334–3340.
54 S. Muromachi, Y. Yamamoto and S. Takeya, *Korean J. Chem. Eng.*, 2016, **33**, 1917–1921.
55 L. Zhao, W. L. Liu, L. D. Zhang, J. S. Yao, W. H. Xu, X. Q. Wang and Y. Z. Wu, *Colloids Surf., A*, 2013, **423**, 69–76.
56 C. Oopathump, O.-U. Kheowan, A. Charoenphakdee, A. Harnwunggmoung, S. M. Smith and C. B. Smith, *Ceram. Int.*, 2017, **43**, 17086–17092.